VI. Conclusions

The *H*-plane coupler-type bend has been found to yield a significant improvement in the performance of double-layer pillboxes as compared to previous designs in terms of reflection and cross-polarization. It has been found that the theory developed in designing the bend is sufficient to enable calculation of the principal dimensions of the bend, requiring only minor adjustments based on measurements for a complete design. The existence of an optimum hole diameter for achieving the shortest coupling length, consistent with a flat frequency characteristic and good directivity, has been hypothesized and verified. Performance of the coupler-type bend has been demonstrated in a wide-angle pillbox model.

VII. Acknowledgment

The work described was performed under the direction of T. W. Madigan of Bell Telephone Laboratories. The coupler-type bend was based on an invention of D. S. Lerner, then at Wheeler Laboratories. The authors wish to thank H. A. Wheeler and N. A. Spencer for their helpful suggestions and guidance. The model of the pillbox used for the measurements was supplied by Bell Telephone Laboratories, who also provided programming assistance and computer time for the calculation of coupler hole patterns.

VIII. References

[1] S. Silver, *Microwave Antenna Theory and Design*. New York: McGraw-Hill, 1949, pp. 460–464. (Single-layer pillbox.)
[2] H. Jasik, *Antenna Engineering Handbook*. New York: McGraw-Hill, 1961, pp. 12–19. (Single- and double-layer pillboxes.)
[3] D. S. Lerner, "Coupler-type bend," U. S. Patent 3 255 456, June 7, 1966.
[4] S. E. Miller, "Coupled wave theory and waveguide applications," *Bell Sys. Tech. J.*, vol. 33, p. 661, May 1954. (Comprehensive treatment of coupling between transmission lines.)
[5] K. Tomiyasu and S. B. Cohn, "The transvar directional coupler," *Proc. IRE*, vol. 41, pp. 922–926, July 1953. (Modal analysis of coupling.)
[6] S. B. Cohn, "Microwave coupling by large apertures," *Proc. IRE*, vol. 40, pp. 696–699, June 1952. (Variation of coupling with frequency for large holes.)
[7] P. W. Hannan and M. A. Balfour, "Simulation of a phased-array antenna in waveguide," *IEEE Trans. Antennas and Propagation*, vol. AP-13, pp. 342–353, May 1965. (Discussion of discrete simulation of periodic structures.)
[8] V. Mazzola, "A wideband tight directional coupler," Polytechnic Institute of Brooklyn, Brooklyn, N. Y., MSEE Rept., 1964.

A Parallel-Plate Waveguide Approach to Microminiaturized, Planar Transmission Lines for Integrated Circuits

HENRY GUCKEL, MEMBER, IEEE, PIERCE A. BRENNAN, AND ISTVÁN PALÓCZ, SENIOR MEMBER, IEEE

***Abstract*—The parallel-plate waveguide with a two-layer loading medium, a conducting semiconductor substrate, and a relatively thin dielectric layer approximates the interconnections in many integrated systems if the fringing fields are ignored. The fundamental mode of this structure is an *E* mode which is a surface wave. Its propagation behavior is analyzed in this paper and the equations are evaluated by highly accurate numerical methods.**

The semiconducting substrate is characterized by its dielectric constant and conductivity. A critical conductivity σ_{min} exists and is related to the cross sectional and material parameters. If the substrate conductivity is given by σ_{min} then the attenuation constant of the line is a minimum. The same value of conductivity yields minimum phase distortion at maximum bandwidth. If the conductivity is larger than σ_{min} the substrate acts as a poor conductor with associated skin effect; if it is smaller, lossy dielectric behavior results.

Analysis shows that it is appropriate to subdivide the frequency range into three intervals. The lowest-frequency interval is characterized by propagation which resembles diffusion. This is caused by the loss in the dielectric layer. The next frequency range extends to some upper frequency which is determined by substrate conductivity and the cross-sectional dimensions. In this interval, the phase velocity of the fundamental mode is controlled by the ratio of dielectric to semiconductor thickness, which, if typical interconnections are considered, implies a very low velocity. This property indicates that the structure can serve as a delay line. Further increases in frequency result in higher phase velocities. Skin effect and dielectric loss behavior describe the propagation in this third interval.

Manuscript received May 23, 1966; revised December 16, 1966.

H. Guckel is with the IBM Watson Research Center, Yorktown Heights, N. Y. He is now on leave of absence to the Dept. of Elec. Engrg. and Computer Components Lab., Washington University, St. Louis, Mo.

P. A. Brennan is with the IBM Watson Research Center, Yorktown Heights, N. Y.

I. Palócz is with the Dept. of Elec. Engrg., New York University, Bronx, N. Y. He was formerly with the IBM Watson Research Center, Yorktown Heights, N. Y.

I. Introduction

LARGE SCALE integration involves a set of interconnected, integrated circuits, which are located on a common semiconductor wafer. The interconnection pattern in most cases serves only as an information link. The desired behavior for an interconnection is a series short circuit. The actual behavior may be obtained if a transmission line representation of the interconnection is available.

A cross section of the type of transmission line which is found in the common substrate system is shown in Fig. 1. The lowest layer is an aluminum metallization which is used for heat transfer purposes. It forms a common ground plane for the transmission system. Its presence reduces the noise coupling between neighboring lines. The silicon layer is the substrate. Its thickness and conductivity are determined by component requirements. The oxide layer insulates the substrate from the transmission line conductor. Its thickness is restricted by fabrication technology.

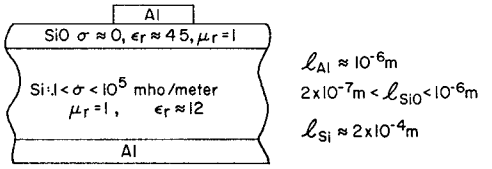

Fig. 1. Interconnection cross section for circuitry on the same substrate with typical thickness dimensions. μ_r and ϵ_r are relative permeability and permittivity.

The resulting transmission line is of the microstrip variety. The loading medium consists of a dielectric and the substrate material with widely varying parameters. Since an exact analysis is not feasible, the choice of an approximate method depends on the intended applications and expected transmission line behavior.

The integrated system which is of interest employs pulse circuitry. The operating frequencies extend from zero to some upper limit, which is determined by the pulse rise-time. Maximum values of three gigahertz are expected. The surge impedance and propagation constant of the transmission line are needed. It appears that an examination of that mode which behaves similarly to the TEM mode in a lossless system would yield the desired information.

The expected transmission line characteristics may be deduced from the following arguments. The structure reduces to microstrip on silicon [1] if the substrate conductivity is small. In this case the oxide layer may be neglected; its thickness is always small compared to the silicon thickness. The method suggested by Wheeler [2] may be extended to describe the lossy dielectric–air microstrip cross section. If the substrate conductivity is high, a TEM perturbation technique may be used [3]. The substrate acts like a lossy ground plane and the oxide becomes the dielectric. The effect of the fringing field will be small since the width of the aluminum conductor is very much larger than the thickness of the oxide.

An exact analysis would therefore involve a microstrip solution with complications. This will not be attempted here. The fringing fields will be ignored. The resulting parallel-plate waveguide [4] exhibits the two loading media, the aluminum conductors, and the air dielectric. The system may be approximated by replacing the aluminum conductors by perfect conductors. This approximation may be compensated for by a standard perturbation correction of the idealized system. The problem may be formulated in terms of the transverse resonance method [5]. The treatment may be specialized to the E modes in view of earlier investigations [6].

The parallel-plate waveguide approximation cannot yield accurate results for the microstrip. However, it will establish qualitative data for all substrate conductivities and will allow a decision on the applicability of either limiting solution.

II. Parallel Waveguide Formulation

The reference directions for the parallel waveguide are given in Fig. 2. The two layers are described by their thicknesses l_1 and l_2, the material constants σ_i—the conductivity of the ith layer, ϵ_i—the relative permittivity of the ith layer, and μ_i—the relative permeability of the ith layer.

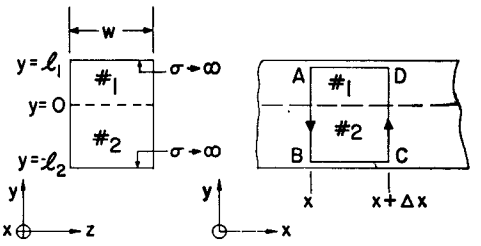

Fig. 2. Idealized cross section and reference coordinates.

The analysis should yield the longitudinal propagation constant γ_x and the driving point impedance Z_0 as functions of the eight parameters and the excitation frequency ω. The driving point impedance is defined as the input impedance of an infinitely long structure. Use of the separation conditions and applications of the transverse resonance procedure for the E mode results in the three eigenvalue equations.

$$\gamma_1^2 + \gamma_x^2 = -k_0^2 \mu_1 \epsilon_1' \tag{1}$$

$$\gamma_2^2 + \gamma_x^2 = -k_0^2 \mu_2 \epsilon_2' \tag{2}$$

$$\frac{\gamma_1}{\epsilon_1'} \tanh \gamma_1 l_1 + \frac{\gamma_2}{\epsilon_2'} \tanh \gamma_2 l_2 = 0 \tag{3}$$

where γ_1 and γ_2 denote propagation constants in the y direction. The primed relative permittivities are defined by $\epsilon_i' = \epsilon_i + \sigma_i / j\omega\epsilon_0$; k_0 designates the quantity $\omega\sqrt{\mu_0\epsilon_0} = \omega/c$; $i = 1, 2$.

The eigenvalue equations may be combined to yield

$$\gamma_x^2 = \frac{j\omega\mu_0 \left(\mu_1 \frac{1}{\gamma_1} \tanh \gamma_1 l_1 + \mu_2 \frac{1}{\gamma_2} \tanh \gamma_2 l_2 \right)}{\frac{\frac{1}{\gamma_1} \tanh \gamma_1 l_1}{j\omega\epsilon_0\epsilon_1'} + \frac{\frac{1}{\gamma_2} \tanh \gamma_2 l_2}{j\omega\epsilon_0\epsilon_2'}} \tag{4}$$

or

$$\gamma_x^2 = \frac{j\omega\mu_0\left(\frac{\mu_1 l_1'}{w} + \frac{\mu_2 l_2'}{w}\right)}{\frac{1}{\frac{j\omega\epsilon_0\epsilon_1' w}{l_1'}} + \frac{1}{\frac{j\omega\epsilon_0\epsilon_2' w}{l_2'}}}. \quad (5)$$

Here w denotes the width of the guide, and $l_i' = 1/\gamma_i \tanh \gamma_i l_i$, $i = 1, 2$, defines two complex quantities, which have the dimensions of length.

Equation (5) lends itself to interpretation in terms of the series impedance and shunt admittance of a T element in an infinite ladder representation of a transmission line. This may be taken to imply that the characteristic impedance of the line is given by (6).

$$Z_0^2 = \left(\frac{\eta_0}{w}\right)^2 (\mu_1 l_1' + \mu_2 l_2')\left(\frac{l_1'}{\epsilon_1'} + \frac{l_2'}{\epsilon_2'}\right) \quad (6)$$

where

$$\eta_0 = \sqrt{\frac{\mu_0}{\epsilon_0}} = 377\ \Omega.$$

This method does not yield an answer to the question of which physical voltages and currents are involved. The driving point impedance involves the total current drawn from the source and includes not only the current which flows on the bounding conductor surfaces but also those currents which are in the conducting loading material. In other words, the representation of a three-component field system by a two-dimensional voltage and current model must be clarified.

In order to resolve this difficulty it is necessary to examine the conversion of the field solutions to the equivalent transmission line. This may be accomplished readily by making use of the perfect conductor boundaries.

The first transmission line equation is obtained by considering the contour *ABCDA* of Fig. 2, for the integration of Maxwell's equations. It yields

$$\frac{\partial v}{\partial x} = -\frac{j\omega\mu_0}{w}\left(\frac{\mu_2}{\gamma_2}\tanh \gamma_2 l_2 + \frac{\mu_1}{\gamma_1}\tanh \gamma_1 l_1\right) i_1 \cosh \gamma_1 l_1 \quad (7)$$

where

$$v(x) \equiv \phi(x, l_1) - \phi(x, -l_2)$$

$$E_y = -\frac{\partial \phi}{\partial y}.$$

The current i_1 is the current which flows on the upper conductor in Fig. 2. A similar expression is obtained if the current i_2 on the lower conductor is considered. In particular, the use of

$$i_x \equiv i_1 \cosh \gamma_1 l_1 = -i_2 \cosh \gamma_2 l_2 \quad (8)$$

leads to

$$\frac{\partial v}{\partial x} = -\frac{j\omega\mu_0}{w}\left(\frac{\mu_2}{\gamma_2}\tanh \gamma_2 l_2 + \frac{\mu_1}{\gamma_1}\tanh \gamma_1 l_1\right) i_x \quad (9)$$

and

$$\frac{\partial i_x}{\partial x} = \frac{-j\omega\epsilon_0 w}{\frac{\tanh \gamma_1 l_1}{\gamma_1 \epsilon_1'} + \frac{\tanh \gamma_2 l_2}{\gamma_2 \epsilon_2'}} v. \quad (10)$$

The current due to the longitudinal field in region #1 may be related to the conductor current i_1 by integrating the current density $J_1 = j\omega\epsilon_0\epsilon_1' E_{x1}$ over the cross section of medium #1, This yields

$$I_1 = -(1 - \cosh \gamma_1 l_1) i_1.$$

The total longitudinal current in medium #1 is therefore

$$I = I_1 + i_1.$$

The same arguments may be applied to medium #2. They lead to a similar result. Thus, i_x is the total current which flows in one of the layers and the conductor associated with the layer. It is therefore a measurable quantity and the use of (6) as a definition of the surge impedance becomes meaningful. A solution of the eigenvalue equations for l_1' and l_2' would yield a useful characterization of the interconnection system.

III. Solution of the Eigenvalue Problem

A numerical solution of the eigenvalue problem may be based on (11) and (12).

$$F_1(\gamma_1, \gamma_2) = \gamma_1^2 - \gamma_2^2 + k_0^2 (r')^2 = 0 \quad (11)$$

$$F_2(\gamma_1, \gamma_2) = \frac{\gamma_1}{\epsilon_1'}\tanh \gamma_1 l_1 + \frac{\gamma_2}{\epsilon_2'}\tanh \gamma_2 l_2 = 0 \quad (12)$$

where

$$(r')^2 \equiv \mu_1\epsilon_1' - \mu_2\epsilon_2'.$$

The Newton-Raphson method was selected to solve the equations. The computations were difficult because a number range of 10^{16} had to be handled. This caused convergence problems due to neighboring roots. In order to avoid this, an estimate of the behavior of the solutions was needed. The lossless case, which is discussed in the Appendix, had to be considered first. It was concluded that the quasi-TEM mode of the lossless system is replaced by the lowest-order surface wave mode in the lossy system. This mode is of interest for wideband applications. Figures 3 to 5 contain data on a fixed geometric arrangement with varying substrate conductivity. They are based on the exact solution of (11) and (12). An interpretation of the data is possible by using approximate solutions to the eigenvalue problem for the lowest-order surface mode.

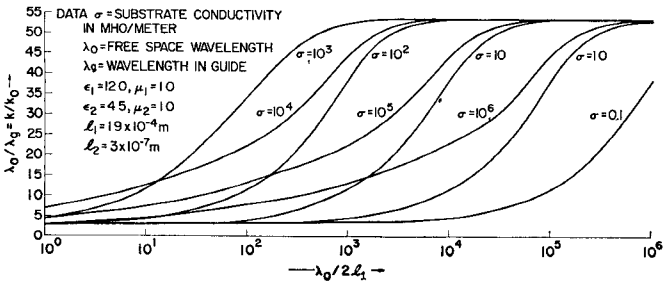

Fig. 3. Dispersion curves for typical integrated transmission lines for several substrate conductivities.

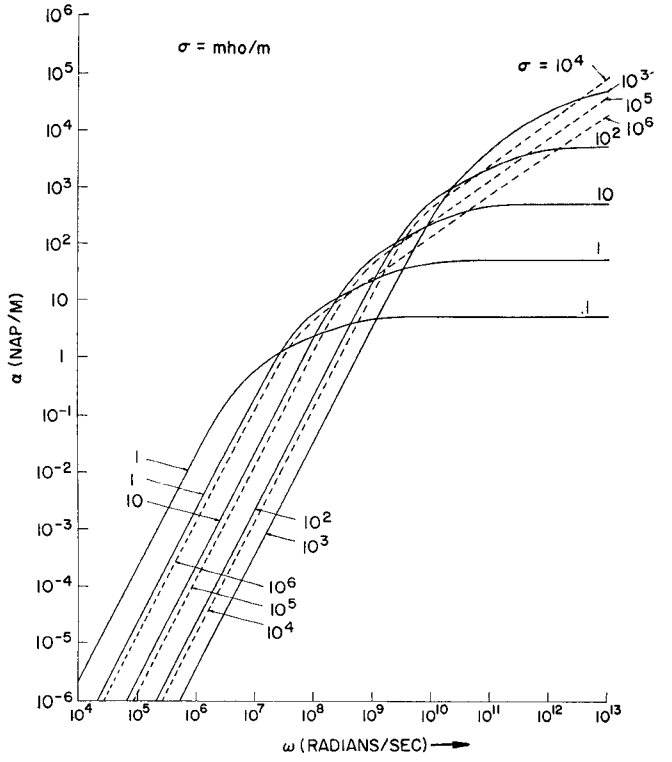

Fig. 4. Attenuation constant associated with the structure used for Fig. 3. The substrate conductivities are in Ω/m.

IV. Approximate Solutions

A numerical solution of the eigenvalue problem yields data for specific applications. In order to study its implications on the general problem, it is necessary to resort to approximate methods. The treatment is specialized to the lowest-order mode.

A. The Low-Frequency Approximation

The condition $l_1' \approx l_1$ and $l_2' \approx l_2$ reduces (5) to

$$-\left(\frac{\gamma_x}{k_0}\right)^2 = \frac{\mu_1 l_1 + \mu_2 l_2}{\dfrac{j\omega\epsilon_0 l_1}{\sigma_1 + j\omega\epsilon_0\epsilon_1} + \dfrac{j\omega\epsilon_0 l_2}{\sigma_2 + j\omega\epsilon_0\epsilon_2}}.$$

The low-frequency limit is therefore given by (13)

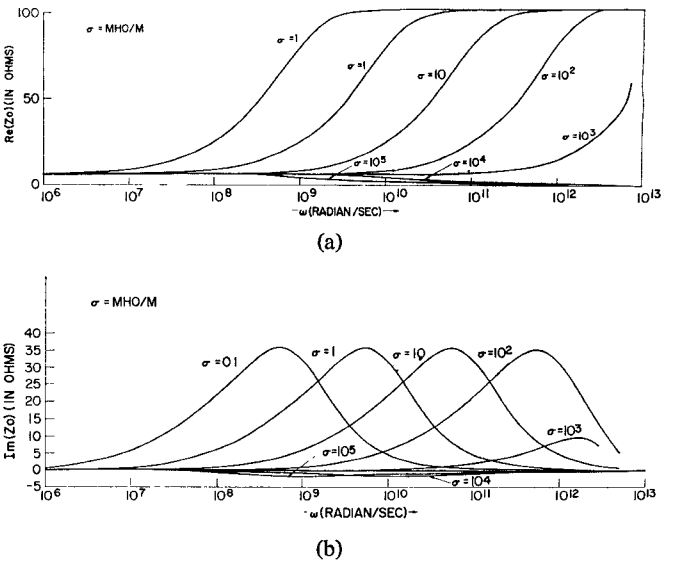

Fig. 5. (a) Real part of the characteristic impedance associated with the data of Fig. 3. The substrate conductivities are in Ω/m. (b) Imaginary part of Z_0.

$$\lim_{\omega\to 0}\left(\frac{\gamma_x}{k_0}\right)^2 = \begin{cases} \dfrac{\mu_1 l_1 + \mu_2 l_2}{\dfrac{l_1}{\epsilon_1} + \dfrac{l_2}{\epsilon_2}} & \sigma_1 = \sigma_2 = 0 \\ -j\infty & \sigma_1 \neq 0,\ \sigma_2 \neq 0. \\ \epsilon_i\left(\mu_i + \mu_j \dfrac{l_j}{l_i}\right) & \sigma_i = 0,\ i \neq j \end{cases} \quad (13)$$

It is also known that the limit is $\mu_i\epsilon_i$ if $\sigma_j \to \infty$ $(i=1, 2;\ i\neq j)$. These two cases were excluded when (4) was formulated. They correspond to the two TEM modes. The low-frequency transmission line network is given in Fig. 6. Equation (13) may be approximated by restricting $\omega \ll \min(\sigma_2/\epsilon_0\epsilon_2, \sigma_1/\epsilon_0\epsilon_1)$. In other words, if both materials behave like metals

$$\gamma_x = 1(+j)\left[\frac{\omega\mu_0(\mu_1 l_1 + \mu_2 l_2)}{2\left(\dfrac{l_1}{\sigma_1} + \dfrac{l_2}{\sigma_2}\right)}\right]^{1/2}. \quad (14)$$

The equivalent transmission line reduces to a *G–L* line if the bounding conductors are perfect. This assumption yields zero attenuation when $\omega = 0$. The phase velocity is finite for all cases discussed in (13). It is zero if $\sigma_1 \neq 0$ and $\sigma_2 \neq 0$, i.e., if real materials are involved, and $\omega = 0$.

The behavior changes when one of the materials behaves like a dielectric. Thus,

$$-\left(\frac{\gamma_x}{k_0}\right)^2 = \frac{\dfrac{\epsilon_2}{l_2}(\mu_1 l_1 + \mu_2 l_2)}{1 + \dfrac{j\omega\epsilon_0 l_1}{\sigma_1}\dfrac{\epsilon_2}{l_2}} \quad (15)$$

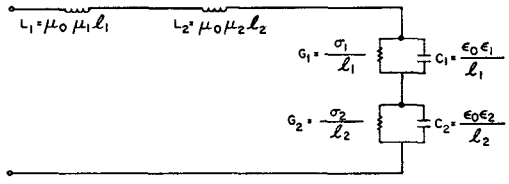

Fig. 6. Longitudinal equivalent for low frequencies.

if

$$\frac{\sigma_1}{\epsilon_0\epsilon_1} > \omega > \frac{\sigma_2}{\epsilon_0\epsilon_2}.$$

A good approximation to (15) with respect to the microstrip parameters of Fig. 1 is given by (16).

$$\frac{\gamma_x}{k_0} \approx j\sqrt{\mu_2\epsilon_2}\left(1+\frac{\mu_1 l_1}{\mu_2 l_2}\right)^{1/2}\left(1-j\frac{1}{2}\frac{\omega\epsilon_0\epsilon_2}{l_2}\frac{l_1}{\sigma_1}\right) \quad (16)$$

if

$$\min\left(\frac{\sigma_1}{\epsilon_0\epsilon_1}, \frac{\sigma_1 l_2}{\epsilon_0\epsilon_2 l_1}\right) > \omega > \frac{\sigma_2}{\epsilon_0\epsilon_2}.$$

Equation (16) indicates that the phase velocity is controlled by the ratio of the two material thicknesses. The condition $l_1 \gg l_2$ applies to the data of Fig. 3. It results in the very low phase velocity of about 1/50 of the speed of light in this particular example. The attenuation depends on the shunt element $R_s = l_1/\sigma_1$. Equation (16) apparently does not include all the losses. A part of the attenuation would have to be proportional to σ_1. A refinement of the expression for the attenuation constant is needed.

B. Second-Order Approximation

The integrated microstrip structure employs dielectric thicknesses of about 0.1 percent of the semiconductor thickness. The approximation $\tanh \gamma l \approx \gamma l$ will therefore first fail for the semiconductor layer or material #1. This would indicate that $\tanh \gamma_1 l_1$ should be approximated by two terms in order to improve the solution. A single eigenvalue equation results:

$$\gamma_1^4 - \frac{3}{l_1^2}\left(1+\frac{\epsilon_1'}{\epsilon_2'}\frac{l_2}{l_1}\right)\gamma_1^2 - \frac{3l_2}{l_1^3}\frac{\epsilon_1'}{\epsilon_2'}k_0^2 r'^2 = 0. \quad (17)$$

The assumptions $\sigma_1 \gg \omega\epsilon_0\epsilon_1 > \omega\epsilon_0\epsilon_2$ and $\sigma_2 \ll \omega\epsilon_0\epsilon_2$ were used to solve (17).

$$\gamma_1^2 = \frac{3\sigma_1}{2l_1^3}\left(\frac{l_1}{\sigma_1}+\frac{l_2}{j\omega\epsilon_0\epsilon_2}\right)\left[1-\left\{1-\frac{4}{3}l_1^3 l_2\frac{\frac{\eta_0^2\mu_1}{\epsilon_2}-j\frac{\omega\mu_0\mu_2}{\sigma_1}}{\left(\frac{l_1}{\sigma_1}+\frac{l_2}{j\omega\epsilon_0\epsilon_2}\right)^2}\right\}^{1/2}\right]. \quad (18)$$

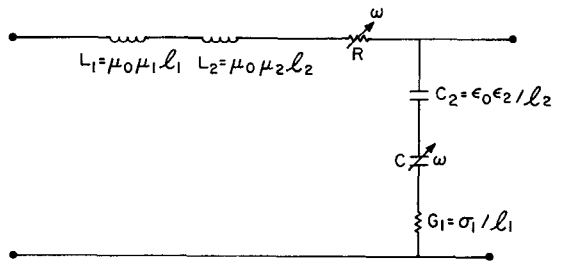

Fig. 7. Low-frequency longitudinal equivalent for metal and dielectric layers. The two frequency-dependent elements are given by

$$R = \frac{1}{\frac{3}{4}\left(\frac{\delta}{l_1}\right)^3\sigma_1\delta} \quad \text{and} \quad C = \frac{3}{2}\left(\frac{\delta}{l_1}\right)^2\frac{\sigma_1}{wl_1}.$$

An evaluation of (18) yields the conclusion that the new value of γ_1 will differ very little from the first-order expression if

$$\omega \ll \frac{\sqrt{3}}{2}\frac{1}{\eta_0 l_1 \epsilon_0}\sqrt{\frac{l_2}{l_1\epsilon_2}}.$$

The data of Fig. 3, which is typical for integrated microstrip, was used to evaluate this inequality. It appears that the low-frequency expression for γ_1 is valid if ω does not exceed a few gigahertz.

The expression for $\tanh \gamma_1 l_1$ may be approximated by two terms. This yields

$$\gamma_x^2 \approx \frac{j\omega\mu_0(\mu_1 l_1+\mu_2 l_2)+\frac{4}{3}\left(\frac{l_1}{\delta}\right)^4\left(\frac{\sigma_1}{l_1}+\frac{j\omega\epsilon_0\epsilon_2}{l_2}\right)^{-1}}{\frac{l_1}{\sigma_1}+\frac{l_2}{j\omega\epsilon_0\epsilon_2}-j\frac{2}{3}\left(\frac{l_1}{\delta}\right)^2\left(\frac{\sigma_1}{l_1}+\frac{j\omega\epsilon_0\epsilon_2}{l_2}\right)^{-1}} \quad (19)$$

where $$\delta = \sqrt{\frac{2}{\omega\mu_0\mu_1\sigma_1}}$$

designates the depth of penetration in material #1.

Equation (19) contains the information which is needed to evaluate the numerical data. It yields the longitudinal equivalent of Fig. 7 if

$$\frac{\sigma_1 l_2}{\epsilon_0\epsilon_2 l_1} > \omega > \frac{\sigma_2}{\epsilon_0\epsilon_2}.$$

It is of interest to note that the equivalent of Fig. 7 can also be obtained from the approximation $|\gamma_1^2| \gg |\gamma_x^2|$. This implies that $\gamma_1^2 \approx j\omega\mu_0\mu_1\sigma_1$, which is the commonly used metallic approximation. Equation (19) yields the desired correction to (16)

$$\frac{\gamma_x}{k_0} \approx j\sqrt{\mu_2\epsilon_2}\left(1+\frac{\mu_1 l_1}{\mu_2 l_2}\right)^{1/2}\left[1-j\frac{\omega}{2}\left(\frac{\epsilon_0\epsilon_2}{l_2}\frac{l_1}{\sigma_1}+\frac{1}{3}\frac{\mu_0(\mu_1 l_1)^2\sigma_1 l_1}{\mu_1 l_1+\mu_2 l_2}\right)\right]. \quad (20)$$

V. The Critical Conductivity

It is evident that the second term in (20) is due to shunt losses and the third due to series losses. Furthermore, it appears that the attenuation constant must attain a minimum with respect to substrate conductivity. If $\mu_2 l_2 \ll \mu_1 l_1$, the conductivity for minimum attenuation is given by

$$\sigma_{\min} = \frac{1}{377}\sqrt{\frac{3\epsilon_2}{\mu_1 l_1 l_2}}.$$

Structures which employ $\sigma_1 > \sigma_{\min}$ will be controlled by the series losses and, conversely, those with $\sigma_1 < \sigma_{\min}$ by the shunt losses. Both types of systems exhibit a propagation velocity which is determined by the geometry. However, the frequency range over which β/k_0 is given by

$$\left(\mu_2\epsilon_2\left(1+\frac{\mu_1 l_1}{\mu_2\epsilon_2}\right)\right)^{1/2}$$

will be quite different. An examination of (19) and (20) results in the conclusion that β will decrease when the real part of (20) is about

$$\frac{\sqrt{3}}{2}\sqrt{\mu_2\epsilon_2}\left(1+\frac{\mu_1 l_1}{\mu_2 l_2}\right)^{1/2}.$$

Thus

$$\beta \approx k_0\sqrt{\mu_2\epsilon_2}\left(1+\frac{\mu_1 l_1}{\mu_2 l_2}\right)^{1/2}$$

if

$$\omega_c > \omega > \frac{\sigma_2}{\epsilon_0\epsilon_2}$$

where

$$\omega_c = \frac{\sqrt{3}}{\dfrac{\epsilon_0\epsilon_2}{l_2}\dfrac{l_1}{\sigma_1}+\dfrac{1}{3}\dfrac{\mu_0(\mu_1 l_1)^2\sigma_1 l_1}{\mu_1 l_1+\mu_2 l_2}}. \tag{21}$$

The ω region in which this expression for β is valid will be a maximum if $\sigma_1 = \sigma_{\min}$. Higher and lower values of σ_1 will decrease the frequency range and increase the attenuation.

VI. High-Frequency Behavior

It is possible to derive some meaningful expressions for the higher-frequency ranges. The interpretation is based on the assumption that l_1 and l_2 are small enough to permit the use of (19). This yields

$$\gamma_x = j\omega\sqrt{\mu_0\epsilon_0\mu_1\epsilon_1}\left(1+\frac{1}{2}\frac{\sigma_1}{j\omega\epsilon_0\epsilon_1}\right) \tag{22}$$

if

$$\sigma_1 < \sigma_{\min} \quad \text{and} \quad l_1 \gg l_2.$$

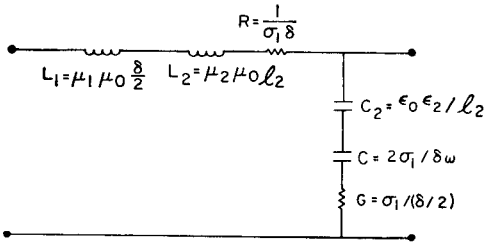

Fig. 8. High-frequency equivalent if $\sigma_1 > \sigma_{\min}$.

This equation describes propagation in a lossy dielectric. It is noted that the real part of (22) is frequency independent. Comparison of (22) with (16) indicates that the loss behavior has reversed. The value of the real part of (22) increases with σ_1.

A similar examination for $\sigma_1 > \sigma_{\min}$ results in the conclusion that these cases are controlled by the skin effect in medium #1. γ_1^2 is essentially equal to $j\omega\mu_0\mu_1\sigma_1$. The expression $\tanh \gamma_1 l_1$ becomes $1+j0$ and

$$\left(\frac{\gamma_x}{k_0}\right)^2 = \frac{l_2\mu_2 + (1-j)\mu_1\dfrac{\delta}{2}}{j\omega\epsilon_0\left(\dfrac{l_2}{j\omega\epsilon_0\epsilon_2}+(1-j)\dfrac{\delta}{2\sigma_1}\right)}. \tag{23}$$

The equivalent circuit associated with (23) is shown in Fig. 8. The rate of increase of the real part of γ_x with respect to ω decreases but does not become independent of ω.

VII. The Characteristic Impedance

The methods of the previous sections may be used to approximate (6). Reference to (20) yields

$$Z_0 \approx \frac{\eta_0}{w}\sqrt{\frac{l_2}{\epsilon_2}}(\mu_1 l_1+\mu_2 l_2)^{1/2} \cdot\left[1+j\frac{\omega}{2}\left(\frac{\epsilon_0\epsilon_2}{l_2}\frac{l_1}{\sigma_1}-\frac{1}{3}\frac{\mu_0(\mu_1 l_1)^2\sigma_1 l_1}{\mu_1 l_1+\mu_2 l_2}\right)\right]. \tag{24}$$

The shunt controlled line exhibits inductive characteristics; the series controlled line has capacitive behavior. If $\sigma_1 = \sigma_{\min}$, the reactive part of the characteristic impedance is a minimum in the low-frequency range. The expression for Z_0 which would correspond to (22) is

$$Z_0 \approx \frac{\eta_0}{w}\sqrt{\frac{\mu_1}{\epsilon_1}}l_1\left(1+j\frac{1}{2}\frac{\sigma_1}{\omega\epsilon_0\epsilon_1}\right) \qquad \begin{matrix}\sigma_1 < \sigma_{\min}\\ l_1 \gg l_2.\end{matrix} \tag{25}$$

If $\sigma_1 > \sigma_{\min}$, (23) may be used to obtain

$$Z_0 = \frac{\eta_0}{w}\sqrt{\frac{l_2}{\epsilon_2}}\left(\mu_2 l_2+\frac{(1-j)\mu_1\delta}{2}\right)^{1/2} \cdot\left(1+\frac{1}{2}(1+j)\frac{\delta}{\sigma_1}\frac{\omega\epsilon_0\epsilon_2}{l_2}\right)^{1/2}. \tag{26}$$

Figure 5 is the exact solution of (6). It appears that the characteristic impedance will initially be controlled by the slow mode and then approach either the TEM mode which would exist in material #2 alone or the TEM mode which would exist in a lossless material with relative dielectric constant $\epsilon_r = \epsilon_1$.

VIII. Imperfect Bounding Conductors

The inclusion of real conductor behavior into the model thus far presented is, in principle, a straightforward process if the transverse resonance method is employed. However, the result is a rather involved set of equations. It is believed that the following method will yield adequate answers for practical purposes.

The surface impedance of a plate of thickness l_σ in air is

$$Z_s = Z_\sigma \frac{Z_{\text{air}} + Z_\sigma \tanh \gamma_\sigma l_\sigma}{Z_\sigma + Z_{\text{air}} \tanh \gamma_\sigma l_\sigma}.$$

If it is assumed that $Z_{\text{air}} \gg |Z_\sigma|$, this expression becomes

$$Z_s \approx Z_\sigma \coth \gamma_\sigma l_\sigma.$$

New values of γ_x and Z_0 are found by adding additional series elements to the longitudinal equivalents. This yields

$$\gamma_x'^2 = \gamma_x^2 + w \sqrt{\frac{j\omega\mu_0}{\sigma}} \cdot \frac{\frac{1}{w_{s1}} \coth \sqrt{j\omega\mu_0\sigma} l_{\sigma 1} + \frac{1}{w_{s2}} \coth \sqrt{j\omega\mu_0\sigma} l_{\sigma 2}}{\frac{l_2}{j\omega\epsilon_0\epsilon_2} + \frac{\tanh \gamma_1 l_1}{\gamma_1(\sigma_1 + j\omega\epsilon_0\epsilon_1)}}$$

$$Z_0'^2 = Z_0^2 + \frac{1}{w} \sqrt{\frac{j\omega\mu_0}{\sigma}} \left[\frac{l_2}{j\omega\epsilon_0\epsilon_2} + \frac{\tanh \gamma_1 l_1}{\gamma_1(\sigma_1 + j\omega\epsilon_0\epsilon_1)}\right] \cdot \left[\frac{1}{w_{s1}} \coth \sqrt{j\omega\mu_0\sigma} l_{\sigma 1} + \frac{1}{w_{s2}} \coth \sqrt{j\omega\mu_0\sigma} l_{\sigma 2}\right]$$

where $l_{\sigma 1}$ and $l_{\sigma 2}$ denote the thicknesses of the upper and lower conductors and w_{s1} and w_{s2} are the effective widths, which, if fringing is ignored, equal w. It is interesting to note that if $\sigma_2 \neq 0$, the above equation yields the following low-frequency limit

$$\lim_{\omega \to 0} Z_0'^2 = \left(\frac{l_1}{w\sigma_1} + \frac{l_2}{w\sigma_2}\right)\left(\frac{1}{w_{s1} l_{\sigma 1} \sigma_1} + \frac{1}{w_{s2} l_{\sigma 2} \sigma_2}\right).$$

The real material assumption ($\sigma_1 \neq 0$, $\sigma_2 \neq 0$, and $\sigma \neq \infty$ for the bounding conductors) yields the proper dc limit.

IX. Conclusions

The lowest-order mode for the two-layer parallel plate waveguide is an E mode which is a surface wave.

If the layers are lossless, the phase velocity of the fundamental mode will be bounded by the phase velocities of the two TEM modes, which occur for the two limiting, homogeneous cross sections. The fundamental mode for the lossless case is commonly called the quasi-TEM mode.

The introduction of losses results in the following:

1) The very low frequencies,

$$\omega \ll \min\left(\frac{\sigma_1}{\epsilon_0\epsilon_1}, \frac{\sigma_2}{\epsilon_0\epsilon_2}\right),$$

propagate in a manner which resembles diffusion. This is caused by the fact that the transverse currents are essentially conduction rather than displacement currents.

2) At slightly higher frequencies, $\omega_c > \omega > \sigma_2/\epsilon_0\epsilon_2$, the transverse displacement current in medium #2 becomes larger than the transverse conduction current in medium #2. A propagation behavior occurs which is based basically on magnetic energy storage in medium #1 and electric energy storage in medium #2. This implies that the two energies are independent in this frequency range and that the phase velocity of the fundamental mode can be controlled by the cross-sectional dimensions.

The frequency range over which this type of propagation occurs depends on the conductivity of the substrate. In particular, it is found that the conductivity value $\sigma_{\min}$ yields a maximum value of ω_c and a minimum value of attenuation. It is found that the attenuation increases with decreasing conductivity if $\sigma_1 < \sigma_{\min}$. The attenuation is proportional to σ_1 if $\sigma_1 > \sigma_{\min}$.

3) If $\omega > \omega_c$ the propagation behavior falls into two classes:

   a) If $\sigma_1 > \sigma_{\min}$ the skin effect of material #1 predominates. The structure behaves as if the substrate forms a lossy conductor for the system. The equivalent circuit exhibits series losses, which exceed the shunt losses. The attenuation increases with decreasing substrate conductivity.

   b) If $\sigma_1 < \sigma_{\min}$ material #1 behaves like a lossy dielectric. Shunt transmission line losses exceed the series losses. The effect of the dielectric layer, material #2, will disappear if its thickness is less than the silicon thickness. An increase of attenuation with increasing conductivity occurs.

The three frequency regions are clearly distinguishable in the exact solutions of the eigenvalue problem. Toe numbers which arise from typical integrated microstrip are somewhat surprising. The phase velocity of the fundamental mode is determined by the ratio of dielectric thickness to substrate thickness. This ratio is about 1/500 for typical integrated microstrip. The resultant phase velocity is $c/50$ if SiO_2 is used as the dielectric. The upper frequency for slow mode behavior, ω_c, is several gigahertz if $\sigma_1 = \sigma_{\min}$. These numbers indicate that the structure is potentially useful as a slow mode delay line. The fact that the phase velocity does depend strongly on the substrate conductivity suggests electronic control of the phase velocity by conductivity control.

Appendix

The Lossless Line

The assumption that the loading media are lossless results in eigenvalues which are either real or imaginary. Propagation along the x direction occurs if $k^2 > 0$ where $k \equiv -j\gamma_x$.

Examination of (3) indicates that $\gamma_1^2>0$ and $\gamma_2^2>0$ cannot be a solution of this equation since $x \tanh x>0$ if $x^2>0$. Thus, two cases must be distinguished:

$$\text{Case I} \quad \gamma_1^2<0 \quad \gamma_2^2>0$$
$$\text{Case II} \quad \gamma_1^2<0 \quad \gamma_2^2<0.$$

A. Case I (Surface Wave)

It is convenient to let $\gamma_1=jk_1$ and $r^2=\epsilon_1\mu_1-\epsilon_2\mu_2$. The use of the defining conditions for this case and $k^2>0$ yields the following bounds on the solutions

$$\epsilon_2\mu_2 < \left(\frac{k}{k_0}\right)^2 < \epsilon_1\mu_1 \tag{27}$$

$$0 < \left(\frac{\gamma_z}{k_0}\right)^2 < r^2 \tag{28}$$

$$0 < \left(\frac{k_1}{k_0}\right)^2 < r^2. \tag{29}$$

Equations (1) and (2) are conveniently combined to yield

$$p^2+q^2=(k_0l_1r)^2 \tag{30}$$

where $p=k_1l_1$ and $q=\gamma_2l_1$. The transverse resonance equation becomes

$$-\frac{p}{\epsilon_1}\tan p+\frac{q}{\epsilon_2}\tanh q\frac{l_2}{l_1}=0. \tag{31}$$

The last two equations may be solved graphically to find corresponding values of p and q. Every possible p must be in the intervals $n\pi\leq p<(2n+1)(\pi/2)$, where $n=0, 1, 2, \cdots$. The integer n is referred to as the order of the mode.

The dispersion relation $\lambda_0/\lambda_g=f(\lambda_0/2l_1)$ is given in parametric form

$$\frac{\lambda_0}{\lambda_g}=\frac{k}{k_0}=\left[\frac{\mu_1\epsilon_1q^2+\mu_2\epsilon_2p^2}{q^2+p^2}\right]^{1/2} \tag{32}$$

$$\frac{\lambda_0}{2l_1}=\pi r\left[\frac{1}{q^2+p^2}\right]^{1/2}. \tag{33}$$

The dispersion curve in the fundamental ($n=0$) mode extends for arbitrary large values of $\lambda_0/2l_1$ (quasi-TEM mode). The graphical analysis indicates that q becomes infinite and p remains finite when $\lambda_0/2l_1\to 0$. Thus, from (32)

$$\lim_{\lambda_0/2l_1\to 0}\frac{\lambda_0}{\lambda_g}=\sqrt{\mu_1\epsilon_1}.$$

This limit is independent of n. Furthermore, since $p\to(2n+1)\pi/2$ as $\lambda_0/2l_1\to 0$ or $\omega\to\infty$, it is easy to show that

$$\lambda_0/\lambda_g\approx\left[\mu_1\epsilon_1-(\tfrac{1}{2}(2n+1)\lambda_0/2l_1)^2\right]^{1/2}$$

when $\lambda_0/2l_1\approx 0$. This implies that

$$\lim_{\lambda_0/2l_1\to 0}\frac{d\left(\frac{\lambda_0}{\lambda_g}\right)}{d\left(\frac{\lambda_0}{2l_1}\right)}=0.$$

The result is again independent of n.

A necessary condition for a mode of order n to propagate is that $p\geq n\pi$. If $p=n\pi$ is substituted into (32) and (33), it is found that $\lambda_0/2l_1=r/n$. The cutoff frequency of the nth mode is therefore given by

$$f_{cn}=\frac{cn}{2l_1r}.$$

In the neighborhood of these points, p is nearly equal to $n\pi$ and q is nearly zero. Then

$$q^2\approx\frac{(k_0l_1r)^2-(n\pi)^2}{1+\frac{l_2\epsilon_1}{l_1\epsilon_2}}$$

$$p^2\approx\frac{(n\pi)^2+\frac{l_2\epsilon_1}{l_1\epsilon_2}(k_0l_1r)^2}{1+\frac{l_2\epsilon_1}{l_1\epsilon_2}}.$$

Substitution into (32) and use of $\lambda_0/2l_1=\pi/k_0l_1$ results in

$$\lambda_0/\lambda_g=\left[\frac{\mu_1l_1+\mu_2l_2-\frac{l_1}{\epsilon_1}\left(\frac{n\lambda_0}{2l_1}\right)^2}{\frac{l_1}{\epsilon_1}+\frac{l_2}{\epsilon_2}}\right]^{1/2}. \tag{34}$$

Thus, if $\lambda_0/2l_1\to r/n$, the value of λ_0/λ_g is

$$\frac{\lambda_0}{\lambda_g}=\begin{cases}\sqrt{\mu_2\epsilon_2} & (n\neq 0)\\ \sqrt{\dfrac{\mu_1l_1+\mu_2l_2}{\frac{l_1}{\epsilon_1}+\frac{l_2}{\epsilon_2}}} & (n=0).\end{cases} \tag{35}$$

Differentiation of (34) with respect to $\lambda_0/2l_1$ and subsequent evaluation at $\lambda_0/2l_1=r/n$ yields

$$\lim_{\lambda_0/2l_1\to r/n}\frac{d\left(\frac{\lambda_0}{\lambda_g}\right)}{d\left(\frac{\lambda_0}{2l_1}\right)}=-\frac{rn}{\sqrt{\mu_2\epsilon_2}}\frac{\frac{\epsilon_2}{l_2}}{\frac{\epsilon_1}{l_1}+\frac{\epsilon_2}{l_2}}. \tag{36}$$

This information was used to construct the upper part of the diagram in Fig. 9. The lowest-order mode ($n=0$) has no cutoff frequency. Equation (35) indicates that it behaves similar to a TEM mode in a uniformly filled guide with effective μ_f and ϵ_f given by

$$\mu_f=\frac{\mu_2l_2+\mu_1l_1}{l_1+l_2}$$

$$\epsilon_f=\frac{\epsilon_1\epsilon_2(l_1+l_2)}{\epsilon_1l_2+\epsilon_2l_1}.$$

These values correspond to energy averaged values [7].

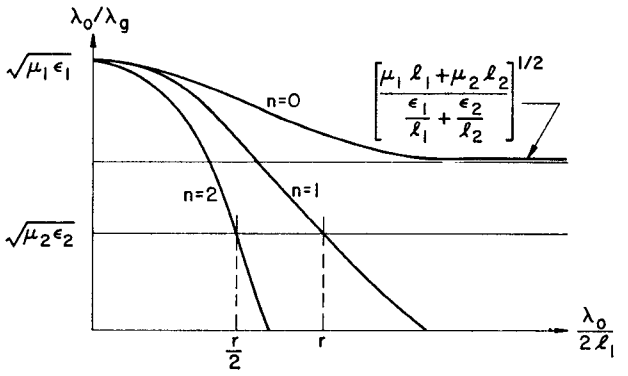

Fig. 9. Dispersion diagram for the lossless case.

Thus

$$\epsilon_f = \frac{\epsilon_1 E_1 + \epsilon_2 E_2}{E_1 + E_2},$$

where E_i=energy/length in the ith region. The nomenclature of quasi-TEM mode is based on these two properties of the fundamental.

B. Case II

The modes which fall into Case II are characterized by $\gamma_1^2<0$ and $\gamma_2^2<0$. Their characteristic equations may be derived from the surface wave equations by replacing q by jq.

$$p^2 - q^2 = (k_0 l_1 r)^2 \tag{37}$$

$$\frac{p}{\epsilon_1}\tan p + \frac{q}{\epsilon_2}\tan\frac{l_2}{l_1}q = 0 \tag{38}$$

$$0 < \left(\frac{k}{k_0}\right)^2 < \mu_2\epsilon_2 \tag{39}$$

$$r^2 < \left(\frac{k_1}{k_0}\right)^2 < \mu_1\epsilon_1$$

$$0 < \left(\frac{k_2}{k_0}\right)^2 < \mu_2\epsilon_2$$

$$\lambda_0/\lambda_g = \sqrt{\frac{\mu_2\epsilon_2 p^2 - \mu_1\epsilon_1 q^2}{p^2 - q^2}}. \tag{40}$$

$$\lambda_0/2l_1 = \pi\sqrt{\frac{\mu_1\epsilon_1 - \mu_2\epsilon_2}{p^2 - q^2}}. \tag{41}$$

The type of solution which occurs is indicated in Fig. 10. In order for the nth mode to propagate, $p \leq n\pi$, $n=1, 2, \cdots$. In the neighborhood of this point $p=n\pi-\delta$, so that there is a smooth transition from surface wave to the Case II mode on the λ_0/λ_g diagram. The lowest frequency for which these modes can propagate is obtained from the condition $\lambda_0/\lambda_g=0$, which results in

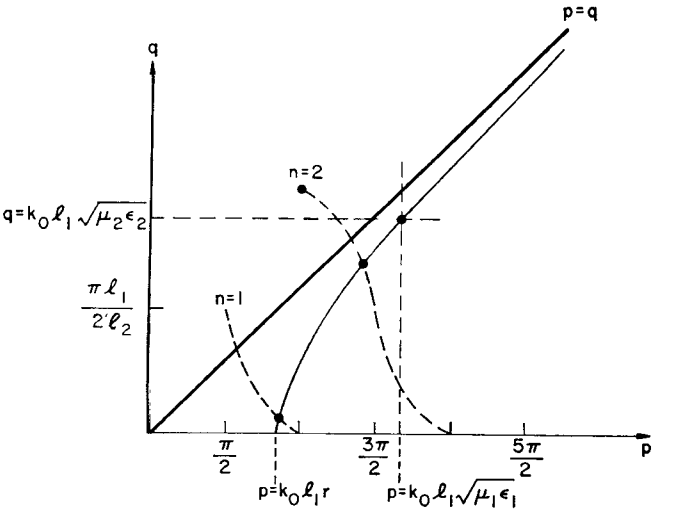

Fig. 10. Graphical solution of (37) and (38).

$$\sqrt{\frac{\mu_1}{\epsilon_1}}\tan(k_0 l_1\sqrt{\mu_1\epsilon_1}) + \sqrt{\frac{\mu_2}{\epsilon_2}}\tan\left(k_0\frac{l_2^2}{l_1}\sqrt{\mu_2\epsilon_2}\right) = 0. \tag{42}$$

Reference to Fig. 10 results in the conclusion that the minimum frequency for n=1 is given by

$$f_{\min} = \frac{1}{4}\frac{c}{l_1\sqrt{\mu_1\epsilon_1}}A$$

where A is a number between 1 and 2. If $l_1/l_2 \gg 1$, A is nearly 2.

Acknowledgment

The authors are indebted to J. C. Dohm and R. S. Warren who provided the structures necessary for experimental verification of the analysis.

References

[1] T. M. Hyltin, "Microstrip transmission on semiconductor dielectrics," presented at the 1965 PG-MTT Symp., Clearwater, Fla., May 1965.

[2] H. A. Wheeler, "Transmission-line properties of parallel strips separated by a dielectric sheet," *IEEE Trans. Microwave Theory and Techniques*, vol. MTT-13, pp. 172–185, March 1965.

[3] H. A. Wheeler, "Formulas for the skin effect," *Proc. IRE*, vol. 30, pp. 412–424, September 1942.

[4] R. E. Collins, *Field Theory of Guided Waves*. New York: McGraw-Hill, 1960, ch. 6.

[5] a) N. Marcuvitz and A. A. Oliner, "Lectures on microwave network theory" (unpublished notes).
b) N. Frank, M.I.T. Radiation Lab., Cambridge, Mass., Rept. T-9, 1942.
c) R. B. Adler, L. T. Chu, and R. M. Fano, *Electromagnetic Energy Transmission and Radiation*. New York: Wiley, 1960, ch. 6.

[6] a) S. A. Schelkunoff, "Anatomy of surface wave," *IRE Trans. Antennas and Propagation*, vol. AP-7, Spec. Suppl., pp. S133–S139, December 1959.
b) H. M. Barlow and A. L. Cullen, "Surface waves," *Proc. IEEE*, vol. 100, pt. III, pp. 329–347, November 1953.

[7] G. A. Deschamps, "Theoretical aspects of microstrip waveguides," *IRE Trans. Microwave Theory and Techniques (Abstract)*, vol. MTT-2, pp. 100–102, April 1954.